

Intercalation as Functional Molecular Dopant for DNA-based Devices

By

Aaron Lincoln Silman
B.S. (University of California, Davis) 2015

THESIS

Submitted in partial satisfaction of the requirements for the degree of

MASTER OF SCIENCE

in

Electrical & Computer Engineering

in the

OFFICE OF GRADUATE STUDIES

of the

UNIVERSITY OF CALIFORNIA

DAVIS

Approved:

Joshua Hihath, Chair

Erkin Şeker

Charles Hunt

Committee in Charge

2016

To my parents for always believing in me and my friends for never allowing me to give up.

“If you wish to make an apple pie from scratch, you must first invent the universe.”

Carl Sagan

Intercalation as Functional Molecular Dopant for DNA-based Devices

ABSTRACT

The biocompatibility, electronic structure, and programmable self-assembly of DNA and RNA systems make them a unique and promising candidate for a variety of single molecule nanodevices and biosensors; yet duplex interactions with foreign molecules that affect said properties have yet to be fully explored. Here I present an investigation into the effects of a Neomycin-Anthraquinone intercalating agent which binds to DNA:RNA duplexes disrupting the electronic structure and possibly allowing for further manipulation of the duplexes electronic properties. The results show a significant increase in conductance from $8.325 \times 10^{-6} \pm 2.69 \times 10^{-6} G_0$ for the DNA:RNA hybrid duplex to a value of $4.962 \times 10^{-3} \pm 1.730 \times 10^{-3} G_0$ for the DNA:RNA hybrid duplex intercalated with the Neomycin-Anthraquinone complex. This corresponds to a conductance increase ratio of 596.03 ± 283.31 caused by the intercalating agent. In addition to the significant conductance increase, the intercalated duplex shows redox properties that are not present before intercalation. These results indicate a promising new technique for doping DNA and RNA systems with intercalating agents which bestow unique behavior.

Acknowledgements

I would first like to thank my advisor Joshua Hihath for his generous mentorship; through him I was challenged to approach every situation critically. I would also like to thank my lab group for their immense kindness and willingness to teach me throughout my time with them.

In addition, I must thank Dev Ayra and his group at Clemson University, South Carolina for synthesizing the intercalator that is explored in this work.

Lastly, would like to extend my most sincere gratitude to Sandia National Laboratories for their generous Critical Skills Master's Program which allowed me to attend the University of California, Davis for my Master of Science Degree.

Thank you all for your help, without it none of this would have been possible.

Table of Contents

1	Introduction	1
1.1	Molecular Electronics.....	1
1.2	Why DNA?.....	2
1.3	Questions Addressed in Thesis	3
2	Electron Transport in Single Molecules	4
2.1	HOMO/LUMO Energy Levels.....	5
2.2	The Landauer Formula	6
2.3	Electron Transport in DNA	8
2.3.1	The Hopping Model.....	8
2.3.2	Hopping Rate	9
2.3.3	Coherence Corrected Hopping.....	12
3	Intercalation	14
3.1	Intercalation Effect on DNA	14
3.2	Anthraquinone-Neomycin Complex	15
4	STM Function	18
4.1	Overview of STM and Operating principles	18
4.2	Scanning Tunneling Microscope Break Junction Technique	20
4.3	Conductance measurements of single molecules.....	22
5	Conductance Modulation of DNA:RNA Hybrid via Intercalation	24
5.1	Preparation of DNA.....	24
5.2	STM-BJ Experimental procedure	25
5.3	Results	28

6	Redox Properties of Intercalated DNA:RNA Hybrid.....	35
7	Conclusion and Outlook.....	39
8	References.....	41

List of Figures

Figure 2.1: HOMO and LUMO Energy Band Diagram	6
Figure 2.2: Hopping model with all hopping rates to nearest neighbors	9
Figure 2.3: Marcus Theory Energy Reorganization	11
Figure 3.1: DPA555 Neomycin-Anthraquinone Intercalator.....	16
Figure 4.1: Overview of STM Components and Operation.....	20
Figure 4.2: STM Break Junction Technique.....	21
Figure 5.1: Substrate Holder Parts.....	25
Figure 5.2: Assembled Substrate Holder	26
Figure 5.3: In-Situ intercalation of DPA555 into DNA:RNA	29
Figure 5.4: DPA555 alone in buffer	31
Figure 5.5: DNA:RNA without linkers.....	32
Figure 5.6: Energy sites after intercalation	34
Figure 6.1: Cyclic Voltogram of DPA555 intercalated DNA:RNA duplex.	36
Figure 6.2: Square Wave Voltogram of DPA555 intercalated DNA:RNA duplex	37
Figure 6.3: Cyclic Voltogram of DPA555 alone	38
Figure 7.1: Possible state resulting from gating intercalated duplex.....	40

1 Introduction

Since the dawn of electronics, we have strived to achieve low power, high speed, and dense packing of devices for computation; and until very recently we have had little problem scaling devices to lower power, higher speeds, and smaller sizes. Modern devices are based around the Complementary Metal Oxide Semiconductor (CMOS) design pattern, which under Moore's "law" has doubled the number of devices on a single chip every two years through a refinement of the lithography processes used in producing these devices. Unfortunately, this law has begun to fail us as we approach the low nanometer scale and current beliefs project even the most advanced lithography will be unable to produce CMOS devices under 5 nanometers that are commercially viable due to the process engineering required¹; even at this feature size some more expensive materials other than traditional silicon may be required. Although many alternative devices have been proposed, molecular electronics stands as one of the best means for extending Moore's law beyond the limit of conventional CMOS.

1.1 Molecular Electronics

Molecular electronics, also called single molecule electronics, aims to replace conventional electronic devices such as wires, transistors, rectifiers, and even entire logic gates with single molecules.

In the late 1940s, Robert S. Mulliken and Albert Szent-Gyorgi advanced the concept of molecular conduction through their work on electron donor-acceptor complexes – also called charge-transfer complexes; this work is often considered the foundation for molecular electronic theory. They subsequently further refined the study of both charge transfer and energy transfer in molecules². In 1974, a paper by Mark Ratner and Ari Aviram illustrated a theoretical molecular

rectifier³, and in 1988, Aviram described in detail a theoretical single-molecule field-effect transistor consisting of a photoconductor coupled to a conductor⁴. Further concepts for single molecule devices, including single-molecule logic gates, were proposed by Forrest Carter of the Naval Research Laboratory at the 1988 conference entitled *Molecular Electronic Devices*⁵. Though these devices were theoretical in nature only, and measurements of the conductance of single molecules did not take place until 1995 by C. Joachim and J. K. Gimzewsky in their Physical Review Letters paper wherein a single C60 molecule was measured⁶. Since then the field has seen large amounts of growth in a relatively short amount of time and many techniques have been developed to probe the device like properties of single molecules. Many molecules have been identified for their device-like properties and experiments continue to reveal and abundance of novel molecules to be explored further.

1.2 Why DNA?

For nearly two decades, researchers have dreamt of exploiting the self-repairing, self-organizing, and self-replication properties of DNA to create nanodevices. DNA is inherently programmable; computational algorithms have been developed to design arbitrary two- and three-dimensional structures from DNA, including polyhedra, smiley faces, and a map of the Americas with a process known as DNA Origami^{7,8}. This allows many interesting structures to be synthesized and tested for unique properties. In addition, despite some structures being of relatively long length studies have shown DNA to conduct charge as efficiently as many other molecular wires⁹.

As early as 1962, Eley and Spivey suggested that the interbase hybridization of π_z orbitals perpendicular to the planes of the stacked base pairs in double-stranded DNA could lead to conducting behavior¹⁰.

Today we have already shown that we can manipulate the unique properties of DNA to create an array of nanostructures for medical applications such as smart drug delivery¹¹ as well as rectifiers¹² and even used as an accurate nanoscaffold for alignment and creation of other higher order nanocircuits¹³.

1.3 Questions Addressed

This thesis looks to explore the effect of an intercalating agent, the Neomycin-Anthraquinone complex, as a ‘molecular dopant’ to DNA and RNA systems. Dopants have always been vital to the creation of bulk material devices and there is evidence that supports molecular dopant structures will be an important factor in the creation of reliable molecular devices. By exploring the effects of novel intercalating agents we expand our knowledge of which properties of molecular dopants may signal usefulness to molecular devices, thereby allowing us to understand which direction we must further explore to continue to expand the field of molecular electronics. In addition, specific questions such as the probable transport mechanism involved in intercalated duplex structures are explored. Thus, the importance of this study is to demonstrate the effectiveness of intercalating agents, particularly the one discussed, as molecular dopants which bestow useful properties to DNA and RNA systems and display the key role they will play in the future of DNA based molecular electronics.

2 Electron Transport in Single Molecules

Classically Ohm's law has been used to describe the electrical conductance of macroscopic materials. The conductance (G) of a material is simply proportional to the cross-sectional area (A), and inversely proportional to its length (L). The full relationship is given by

$$G = \frac{\sigma A}{L}$$

where σ is the conductivity of the material which can be measured experimentally and is dependent on the charge carrier density and mean free path of the charge carriers. Though, as the conductor's size is reduced several effects which were negligible on macroscopic scales become increasingly significant for characterizing the conductance of nanoscale conductors; thus, when a conductor's feature size is on the scale of nanometers the electron transport cannot be accurately modeled with Ohm's Law. For instance, as the length of the conductor becomes smaller than the mean free path of the carriers there will be no scattering during transport through the conductor. As a result, the carrier transport cannot be described by a diffusive process which Ohm's Law assumes. Instead the transport is better described by the ballistic transport regime, where carriers do not experience scattering due to impurities in the material, local defects, or lattice vibrations. Second, the contact resistance between macroscopic electrodes and the nanoscale conductor strongly affects the overall conductance; whereas before this resistance was negligible to the overall resistance of the system. Third, nanoscale objects have a quantized excitation spectrum, as opposed to a band of excited states such as in a bulk semiconductor. This affects how many carriers can be excited – and thus mobile – at one time. In addition to these there are many other specific corrections depending on the system that need to be accounted for to correctly model

carrier transport in nanoscale systems. To understand how one might more accurately describe such a system it is important to understand how excited carriers behave in molecular systems.

2.1 HOMO/LUMO Energy Levels

Macroscopically, carriers transport charge in inorganic semiconductors through the valence and conduction bands, for holes and electrons as charge carriers, respectively. The phenomena of valence and conduction bands comes about as a result of bulk material properties; since individual molecules do not share these bulk properties one must consider transport through another means. Just as in bulk semiconductors where the valence band represents the electronic states that are filled in a non-excited (ground) state, in any molecule there exists molecular orbitals that are fully occupied in the ground state, the highest in energy of this group of occupied orbitals we prescribe the phrase Highest Occupied Molecular Orbital (HOMO) and is analogous to the valence band edge. Similarly, just as the next available state that carriers can occupy above the valence band in bulk semiconductors is the conduction band, the next available molecular orbital that electrons in a molecule can occupy is prescribed as the Lowest Unoccupied Molecular Orbital (LUMO) and represents an excited state of the molecule; these two states are shown in Figure 2.1.

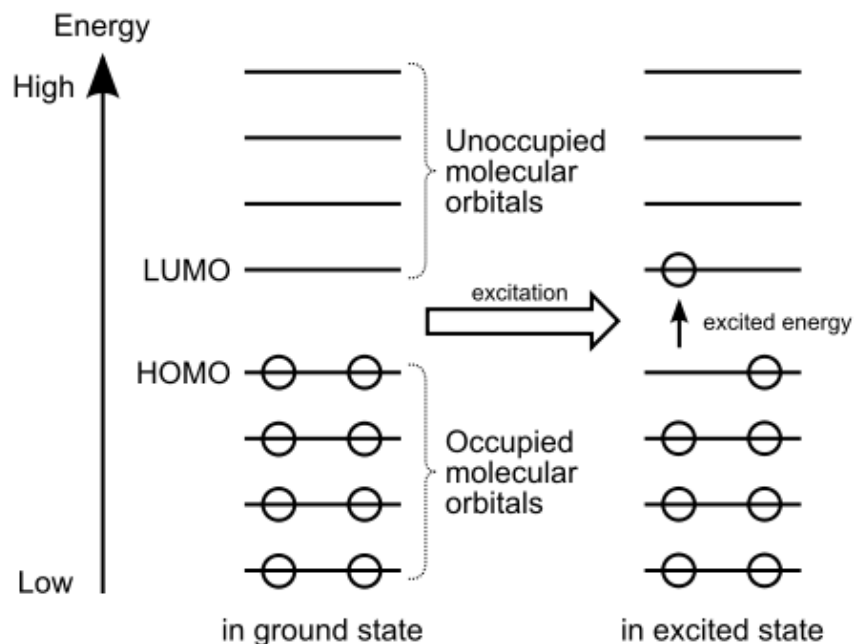


Figure 2.1: HOMO and LUMO Energy Band Diagram
 Image used with permission (reference 14)

Transport takes place via the HOMO and/or LUMO energy levels as these energy levels are the closest to the fermi level of the electrodes on either side when contact is made to the molecule as it reorganizes to the pinned fermi level. Understanding the HOMO/LUMO system is vital to creating a model that can accurately describe charge transport in molecular devices such as DNA. In addition to this, a conductance model such as the Landauer model is introduced to describe a molecular junction's conductance.

2.2 The Landauer Formula

In order to overcome the challenges posed by Ohm's law at the ballistic transport regime we introduce the Landauer formula. Named after Rolf Landauer who first suggest the form of the equation in 1957¹⁵, the formula relates the electrical resistance of a quantum conductor to

the scattering properties of the conductor. In its most simple case, where the quantum conductor has two terminals (such as a wire) the scattering matrix is given by:

$$G(\mu) = G_0 \sum_{n=1}^N T_n(\mu)$$

where G is the electrical conductance, G_0 is the conductance quantum, a constant that is equal to $2e^2/h$ and represents the conductance of a perfect molecular wire with a single transmission channel, μ is the chemical potential, and T_n is the transmission eigenvalues of all transport channels in the conductor; the summation is over all transport channels. Physically this makes sense, it simply states that the conductance of the of nanoscale conductor is given by summing the transmission probabilities an electron has when propagating through a material with energy equal to its chemical potential μ ¹⁶. An important note to understand is that the conductance quantum G_0 is not the smallest unit of conductance but rather the conductance of a single perfectly transmitting channel, that is, a channel where every injected electron moves through to the other side without reflection. Typically, a single line of metallic atoms (such as gold) provides a single perfectly conducting channel, but if the line of metallic atoms is replaced with a molecule bound to electrodes on either side it is feasible that some carriers enter, spend time in along the molecular ‘bridge’ and return to the electrode they entered from. To understand how this is possible I introduce the hopping model, a common transport model used to describe carrier transport through single molecules and the leading model to describe transport in DNA systems.

2.3 Electron Transport in DNA

2.3.1 The Hopping Model

The question of whether and how electrons migrate over long distances through DNA was raised over 30 years ago, and is still a matter of controversy¹⁷. Coherent tunneling and incoherent hopping have emerged as the mainstream theories to explain short-range and long-range charge transport in DNA, respectively¹⁸. Hopping, a type of diffusive, incoherent transport, is the combination of multiple superexchange steps, or “hops”, in which the charge occupies space on intermediate energy “bridge” sites along the length of the molecule¹⁸; this process is shown in Figure 2.2. Although, superexchange has a strong distance dependence, hopping has a much smaller one; this is somewhat intuitive because very long super-exchange steps are avoided by allowing for multiple much smaller hops to each bridge site¹⁹.

For DNA systems hopping has been shown to be the most likely long-range transport mechanism through a series of conduction experiments performed by the Tao group²⁰ as well as a variety of confirmatory experiments done by the Hihath group^{21,22}. Based on the findings from publications that work with dsDNA and DNA:RNA molecular electronic system the hopping model is the most fit to describe the system explored in this study.

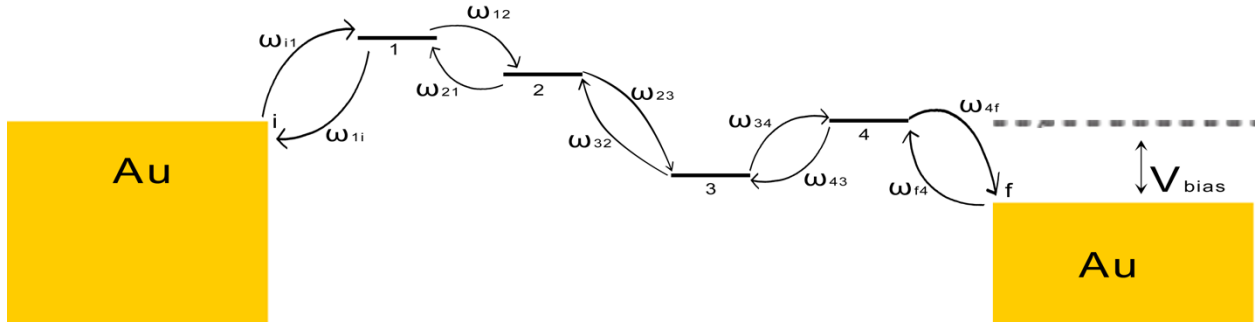


Figure 2.2: Hopping model with all hopping rates to nearest neighbors. “Backwards hops” are statistically unfavorable due to the applied bias.

2.3.2 Hopping Rate

In order to establish the conductance of a system wherein hopping transport is the primary means of electrical conduction it is useful to know the rate at which carriers hop along the bridge sites of the molecule. One can intuitively set up this problem as follows:

First we establish the probability rate of site i being occupied as

$$\frac{\partial f_i(t)}{\partial t} = f_i(t) (1 - f_j(t)) \omega_{ij} - f_j(t) (1 - f_i(t)) \omega_{ji}$$

where f_i is the probability that state i is occupied, ω_{ij} is the rate at which hopping occurs from i to j ²³. Using μ_i as the chemical potential of the molecule at bridge site i and E_i as the energy of bridge site i the occupational probability f_i is simply given by the Fermi-Dirac distribution

$$f_i = \frac{1}{1 + e^{\frac{E_i - \mu_i}{k_b T}}}$$

Assuming no correlations between the occupation probability of different localized states, the steady-state current between these two sites is given by

$$I_{ij} = q \left[f_i(t) (1 - f_j(t)) \omega_{ij} - f_j(t) (1 - f_i(t)) \omega_{ji} \right]$$

At this point one must consider the transition rate ω_{ij} in order to fully determine the hopping rate current. Two common rates have been developed and are often used, the Miller-Abrahams rate and the Marcus rate. The Miller-Abrahams rate is given by

$$\omega_{ij} = v_0 \begin{cases} e^{-2\gamma r_{ij} + \frac{\Delta E_{ij}}{k_b T}} & : \Delta E_{ij} = E_i - E_j \geq 0 \\ e^{-2\gamma r_{ij}} & : \Delta E_{ij} = E_i - E_j \leq 0 \end{cases}$$

where v_0 is a material specific rate constant, r_{ij} is the distance between the bridge sites i and j , and γ is an inverse localization radius describing the decay of transfer integrals. One immediately notices that the site-energy difference ΔE_{ij} is present such that an ‘‘hop uphill’’ (endothermic transfer) is energetically unfavorable. Although this hopping rate includes some of the key parameters such as transfer integrals and site-energy differences necessary to determine the hopping rate of a molecular system, the main disadvantage of the Miller-Abrahams rate lies in the fact that experimental data is necessary for its parametrization, and therefore it cannot be used to predict mobilities²³. In addition to this, many molecular details are neglected.

Many alternatives to the Miller-Abrahams hopping rate have been suggested. Here we consider the high temperature limit of the classical charge-transfer theory proposed in the 1950s by Rudolph A. Marcus. Incidentally, this equation came about as a general way to explain the rates of electron transfer during chemical reactions, specifically the rate at which an electron can move or jump from one chemical species to another and was originally formulated to address outer sphere electron transfer reactions, in which the two chemical species only change in their charge with an electron jumping, but do not undergo large structural changes²⁴.

Despite being significantly more computationally demanding, the Marcus rate allows one to link the chemical and electronic structure, as well as the morphology, to charge dynamics and, in principle, provide a route for predicting charge transport without experimental input. The

equation Marcus proposed for the hopping rate, ω_{ij} , from site i to site j across the distance r_{ij} is given by

$$\omega_{ij} = \frac{2\pi}{\hbar} [H_{ij}]^2 \frac{1}{\sqrt{4\pi\lambda k_b T}} e^{-\frac{(\Delta G_{ij} + \lambda)^2}{4\lambda k_b T}}$$

where $[H_{ij}]^2$ is the transfer integral obtained from the overlap of the wavefunctions between sites i and j and which is proportional to the tunneling contribution, λ is the reorganization energy (the energy required to "reorganize" the system structure without making charge transfer) which has two contributions $\lambda = \lambda^{int} + \lambda^{out}$ from intramolecular reorganization and from outer-shell reorganization, $k_b T$ is the thermal energy (k_b is the Boltzmann constant and T is the absolute temperature), and ΔG_{ij} is the energy difference between sites i and j ²⁴. In Figure 2.3 one can see the how a systems energy is reorganized through the charge transfer process.

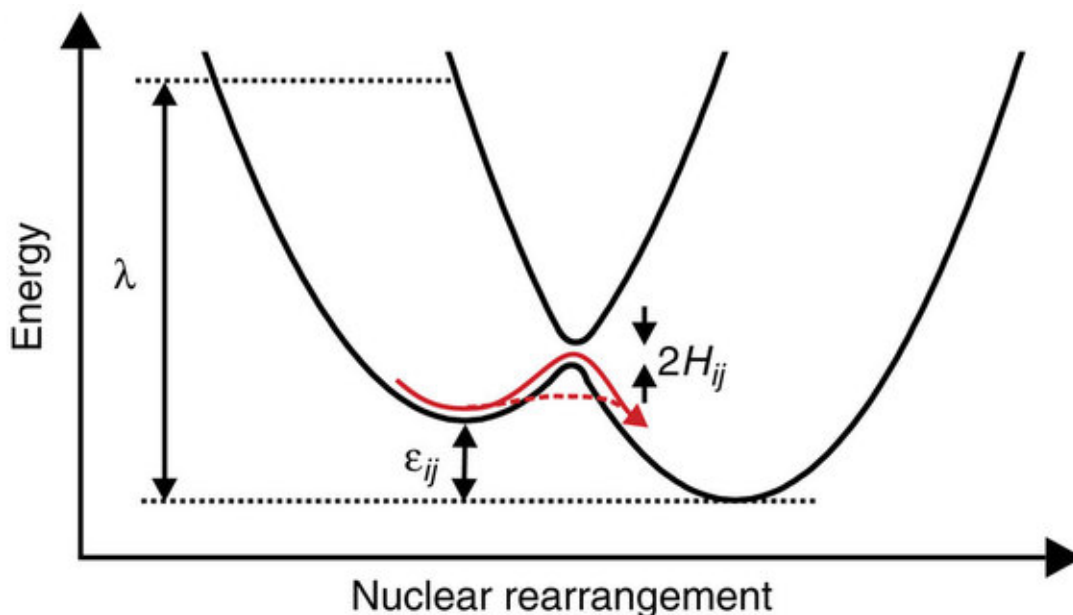


Figure 2.3: Marcus Theory Energy Reorganization
 Diagram shows the reorganization of energy caused by electron transfer.
 Image used with permission (reference 25)

The hopping rate is important because it gives one an easier way to determine the conductance of a molecular system by calculating the current through hopping sites. From the current one can find the conductance as

$$\sigma_{ij} = \frac{I_{ij}}{\Delta\mu_{ij}}$$

In addition to this one could use the Landauer Model to estimate the conductance of the molecular system by knowing the probabilities for carriers to hop from each bridge site. Using these a total probability can be calculated for a carrier to make it through to the exit electrode and thus a transmission probability is obtained. When there is only one path for the carriers to transport across (assuming nearest neighbor hopping only) this total probability gives a direct conductance as a percentage of the quantum conductance G_0 .

2.3.3 Coherence Corrected Hopping

Hopping is an incoherent transport because it relies on energy typically imparted by phonons to allow for carriers to hop from one bridge site to another of slightly higher energy. Because the transport is incoherent the carriers lose information about their phase with each hop. In 1988, Marcus Buttiker introduced a model wherein a coherence correction factor is applied to a system thought to have entirely incoherent transport²⁶.

Consider now the situation in which some carriers can execute one or more full revolutions at a bridge site before losing phase memory. We can then expect a small correction to the hopping transport by a term which depends on the phase $\phi = kw$ accumulated at the bridge site. In addition to this, if a set of bridge sites electronic structure becomes very delocalized it allows for large overlap between the wavefunctions. This, in turn, allows for small inelastic hops between bridge sites and thus a preservation of phase through the transport²⁶. Thus, this

'coherence corrected hopping' can come about due to a delocalization of the molecular orbitals across a hopping system.

This is important to note due to the possibly large increase in hopping rate and thus conductance. As will be discussed later, the large increase in conductance due to the introduction of the intercalator into the DNA system could be understood with this coherence corrected hopping model instead of a traditional thermally activated hopping model. A transition from the latter to the former could explain the large transition in conductance.

3 Intercalation

Intercalation occurs when molecules of an appropriate size and chemical nature fit themselves in between base pairs of DNA. These ligands are mostly polycyclic, aromatic, and planar, and have found uses in staining. Intensively studied DNA intercalators include berberine, ethidium bromide, proflavine, daunomycin, doxorubicin, and thalidomide²⁷. This study aims to further explore anthroquinone as an intercalating agent by combining it with the major groove binder neomycin which allows for a stabilizing effect on the entire DNA-Intercalator structure.

3.1 Intercalation Effect on DNA

In order for an intercalator to fit between base pairs, the DNA must dynamically open a space between its base pairs by unwinding, the degree of unwinding varies depending on the intercalator. This unwinding causes the base pairs to separate, creating an opening for the intercalator to bind. These structural modifications can lead to drastic functional changes in the DNA. For example, in a biological system intercalators often inhibit DNA transcription and replication as well as DNA repair processes which make intercalators potent mutagens²⁸.

Electronically, intercalators have been shown to reorganize the electronic density along the length of the π -stack – the ‘stack’ of molecular orbitals formed by the alignment of the base pairs – which can increase or decrease the conductance of the DNA²⁹, as well as bestow certain device properties such as rectification that the DNA does not display on its own¹².

In one study by Wang et al.²⁹ intercalators were used to modulate the conductance of DNA to varying degrees based on the number of intercalators between the base pairs of the DNA. Using both Ethidium Bromide (EB) and SYBR Green 1 (SG) as representative intercalators for two binding modes – classical intercalation between base pairs for EB or major groove binding

for SG – they found that the intercalation processes lead to profound changes in the structural integrity of DNA, such as stabilization, lengthening, stiffening, and unwinding of the double helix. In turn, these structural changes accounted for a large decrease in conductivity due to the breaking of the π -stack. They show that the DNA conducts at three different values depending on the length of exposure to the intercalator. The DNA has three locations which the intercalator may occupy simultaneously, resulting in three conductance values depending on the number of intercalators present in the DNA.

Moreover, Guo et al has shown that by studying the binding affinity of the intercalating agent coralyne, one can synthesize DNA which controls where along the base pair stack the intercalator binds to, producing an asymmetric molecule that behaves as a molecular rectifier with a rectification ratio of 15^{12} .

Clearly the introduction of intercalating agents to DNA based devices is a promising effort towards the creation of molecular devices with various purposes. This study aims to explore the potential for a new intercalating agent to be used in DNA:RNA based devices.

3.2 Anthraquinone-Neomycin Complex

The Anthraquinone-Neomycin complex (also referred to as DPA555) shown in Figure 3.1 is a base-pair stack intercalator (anthraquinone) bound via a molecular chain to a major groove binder (neomycin). By forming this complex, the neomycin acts as an anchor that forces the anthraquinone into a preferential binding position in the DNA π -stack. It has been shown that these complexes have a propensity towards binding to A-form duplexes³⁰, thus a DNA:RNA hybrid is useful to use to explore this intercalator since they always take the A-form conformation.

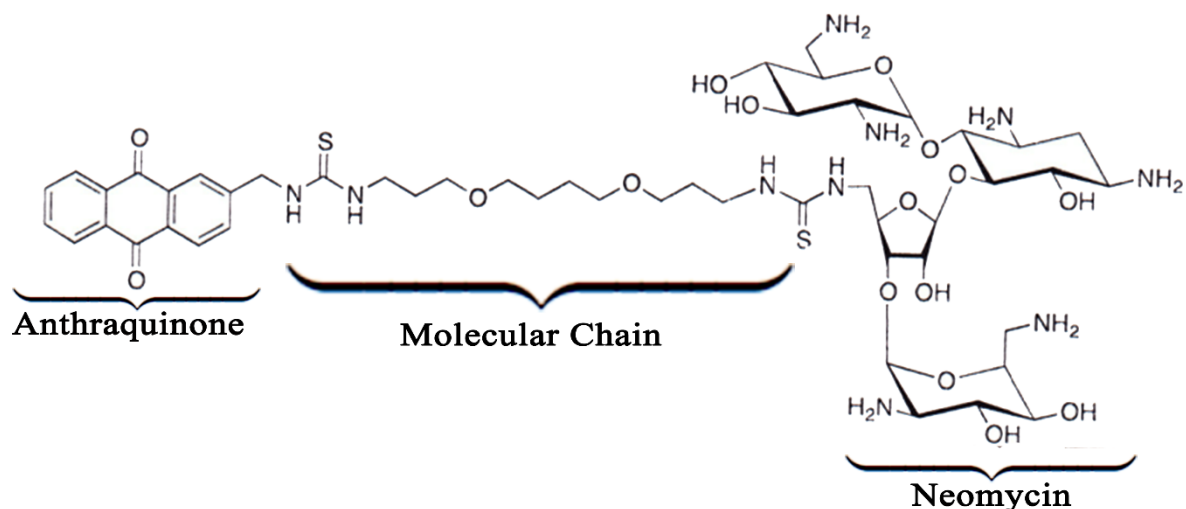


Figure 3.1: DPA555 Neomycin-Anthraquinone Intercalator

Neomycin is an aminoglycoside which has shown strong binding affinity to structures containing RNA³¹. Not only has it shown increase thermal stability large nucleotide structures such as DNA:RNA triplex structures³², it allows for a more consistent binding affinity for attached intercalators to bind into the duplex structure³³.

Anthraquinone was chosen as the attached intercalator due to its proven redox capabilities³⁴ and its known ability to intercalate between the base pairs in duplex structures³⁵. First, the ability to intercalate between bases, disrupting the π -stack, may prove useful as providing an additional energy site for hopping to occur or potentially delocalizing the bases molecular orbitals allowing for stronger overlap. These two factors can contribute to how transport is carried out in a hopping system and can affect the conductance greatly. Second, the redox capabilities of the intercalator are of particular interest due to the possibility to allow manipulation of its electronic structure through an externally applied gate. Given its reduction and oxidation potentials one could theoretically gate the intercalated anthraquinone to modulate the electron density of the π -stack, if the resulting change in the conductance is large it makes it suitable for many

nanobiotechnology and molecular device applications. It has already been shown that single anthraquinone molecules can be gated to their reduction and oxidation potentials in order to modulate the quantum interference disrupting charge transport³⁴; thus by incorporating this effect into DNA based systems which are good candidates for molecular electronics due to their self-assembly properties, transistor-like behavior may arise by applying the external gate to push the anthraquinone into reduction and oxidation states which modulate the conductance.

This study aims to further explore the effects of this intercalator on DNA:RNA duplex structures, particularly we aim to identify the electronic changes induced by this unique molecule, understand how it affects transport through the system, and explore how one might use the intercalator to impart device like characteristics to DNA systems.

4 STM Function

Conductance traces reported in this thesis were acquired using a Scanning Tunneling Microscope (STM) using the Scanning Tunneling Microscope Break Junction (STM-BJ) methodology. The measurements were all performed at room temperature using a PicoSPM STM head (Molecular Imaging) in conjunction with a Nanoscope E controller (Digital Instruments). In this chapter, the basic operating principles of the STM are described as well as the STM Break Junction technique used to measure transport through single gold-molecule-gold junctions.

4.1 Overview of STM and Operating principles

A scanning tunneling microscope is an instrument for imaging surfaces at the atomic level. It was developed in 1981 by Gerd Binnig and Heinrich Rohrer at IBM in Zurich³⁶. To image a sample a conducting tip is brought very near to the surface to be examined, a bias applied between the two allow electrons to tunnel through the vacuum between them. The resulting tunneling current is a function of tip position, applied voltage, and the local density of states (LDOS) of the sample. As a result, one can perform analysis on the current measurements to characterize both the surface topography and electrical topography of the sample³⁷. Although traditionally performed in vacuum, an STM can be used to analyze surfaces in air, water, and various liquid and gas environments; and can operate at temperatures near zero kelvin to hundreds of degrees Celsius.

To acquire measurements from the STM, first a sharp probing tip cut from gold is placed in the STM head and a conductive substrate one wishes to measure is placed under the probing tip. A bias is applied to the substrate to encourage tunneling to the tip. A coarse position adjustment motor brings the substrate to within tunneling distance of the tip. When the current

set point has been reached via the coarse adjustment the probing tip is then finely adjusted via a piezoelectric element to ensure the tip does not “crash” into the substrate while scanning the surface. In order to acquire high resolution measurements from the STM a piezoelectric-based scanning unit which allows for sub-angstrom control of the probing tip in all three Cartesian directions is used to scan the surface. Within the STM head there is an amplifier circuit which amplifies the current measurement from the substrate to the tip which are to be analyzed further.

Lastly, a feedback loop is present to control the piezoelectric element as it scans so that it may be in one of two modes: constant current, in which the piezoelectric element moves the probing tip to maintain a constant tunneling current throughout the substrates topography; and constant height, in which the probing tip is kept at a constant height and fluctuations in current allow for detail to be given about the surface topography. This feedback loop for STM operation is presented in Figure 4.1.

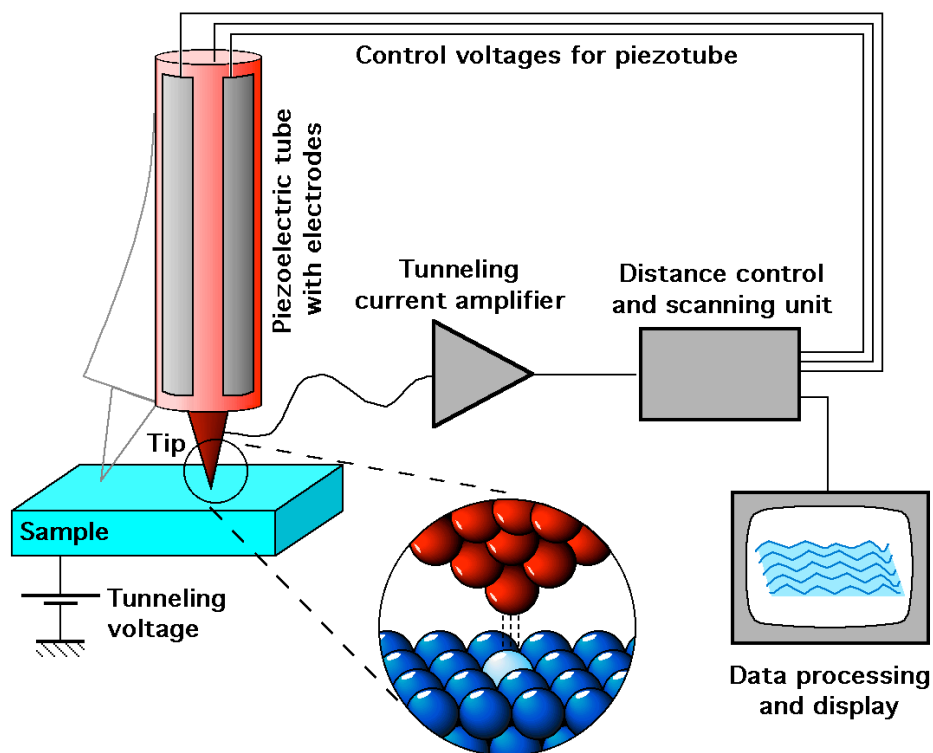


Figure 4.1: Overview of STM Components and Operation
 As the tip of the STM scans back and forth the tunneling current from the surface to the tip is recorded. A control unit analyzes the data in a feedback loop which controls the tip heads height and movement and the data captured is processed and plotted on screen.

Image used with permission (reference 38)

4.2 Scanning Tunneling Microscope Break Junction Technique

The Scanning Tunneling Microscope Break Junction (STM-BJ) Technique is a procedure for studying electron transport through single molecules. It was developed by Xu et al., in 2003³⁹ and continues to this day to be the backbone for finding the conductance of a single molecule.

In this technique, a metallic substrate and probe tip (typically gold for both) are used. A solution is placed over the substrate which has the desired molecule dissolved into it. The subject molecule contains two or more linker groups which will bind to both the substrate and tip

(typically either thiol or amine groups) and the molecule is given time to bind to the substrate without the tip present to create many molecules bound to the surface of the substrate.

The molecular junction is formed by bringing the tip very close to the gold – often “crashing” the tip into the gold – and pulling the tip away. As the tip moves away one of the linker groups on a molecule bound to the gold substrate also binds to the probing tip which allows for the passage of current through the molecule (which was previously transported through tunneling). This entire system of electrode-molecule-electrode is referred to as a molecular ‘junction’ and the process of repeatedly ‘tapping’ the surface to create molecular junctions is shown in Figure 4.2a.

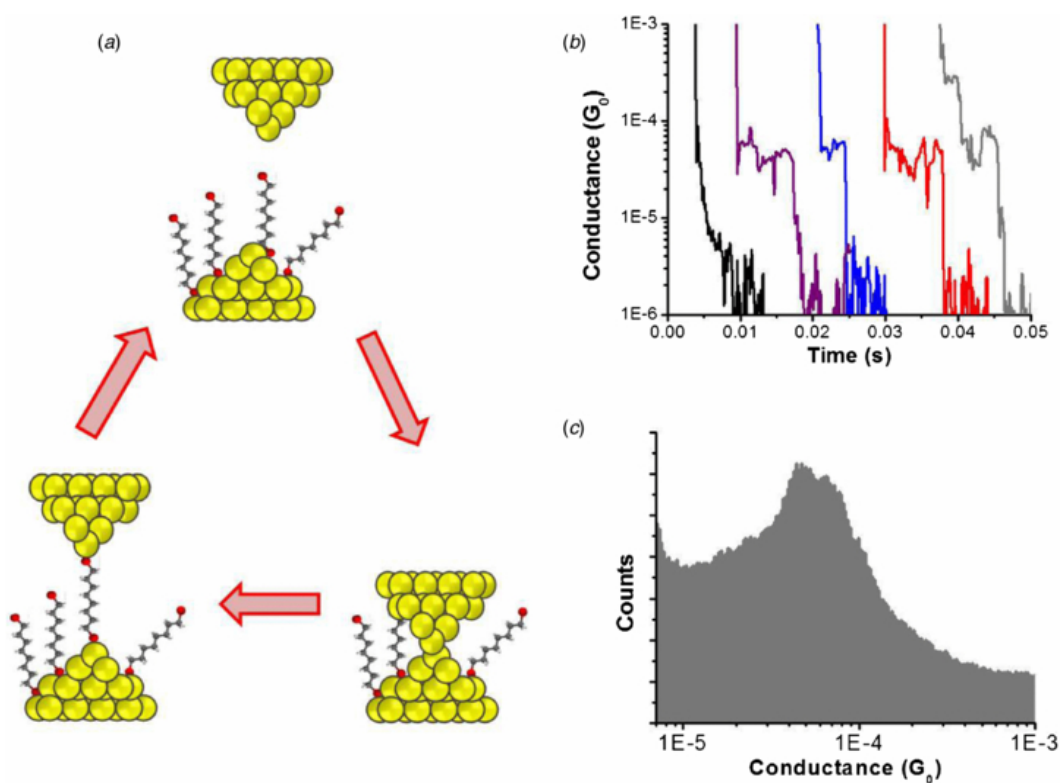


Figure 4.2: STM Break Junction Technique

(a) Piezoelectric element moves gold tip up and down onto substrate with molecules, current measurements are taken throughout. When a molecule is present in the junction a conductance “step” is shown such as in (b). Each conductance trace with a step is selected and a histogram (c) is generated from these step-like curves resulting in the statistically likely conductance of the molecule.

Image used with permission (reference 40)

Current measurements are made throughout the entirety of this process and the resulting current trace is saved for processing. When a molecule does not bind between the gold tip and substrate the current trace will decay from the quantum conductance to below the detection limit in a smooth exponential. If one or more molecules are trapped between the gold tip and substrate one will observe a noticeable “step” in the current trace as shown in Figure 4.2b. One can determine how many molecules formed the junction by counting the number of ‘steps’ on the current trace. This step occurs for a short time while the tip is pulling away and when the distance grows too large the molecular junction is broken and the exponential decay to below the detection limit ensues.

4.3 Conductance measurements of single molecules.

Small changes in the binding site, binding angle, molecular configuration, strain and various other parameters can affect the transport properties of the molecular junction. As a result, multiple thousands of conductance curves are collected during one experiment. In doing so, one can create a histogram that statistically depicts the most likely conductance for transport through a particular molecular junction.

For each break-junction experiment performed, between 3,000 and 6,000 current-distance traces were acquired from the STM. From these traces, about 5 to 15% showed steps corresponding to a molecular junction. An automated selection process in LabVIEW takes all the acquired curves during a break-junction experiment and filters out the ones with no steps. In the current filtering LabVIEW program, each current trace was fitted by linear regression using LabVIEW’s built-in Curve Fitting VI function. This VI would give a best fit for a typical current curve and would assign a residual value to it. The curve was rejected if its residual value fell below a specified cutoff value inserted in the front panel of the program.

After filtering out current-distance traces which do not show signs of a molecular junction, i.e., no ‘step’ in the trace, a histogram must be constructed. First the LabVIEW program converts the current-distance traces into conductance-distance traces using the known applied voltage V , the measured current from the STM I , and the equation $G = I/V$. Next a 1D histograms of conductance traces like the one shown in Figure 4.2c is created. All the conductance value data points measured along a conductance-distance traces are binned into a histogram along the conductance axis. A small bin size is used to resolve sharp conductance peaks as well as multiple separate conductance peaks that are very close together.

The conductance histograms were fit with a Gaussian equation using Origin Pro 9 data analysis and graphing software to extract the most probable conductance value, i.e. the peak of the histogram. Origin’s Gaussian Peak fitting function is described by

$$y = y_0 + \left(\frac{A}{w \sqrt{\frac{\pi}{2}}} \right) e^{-2 \left(\frac{x-x_c}{w} \right)^2}$$

Where y is the fit the histogram counts in the bin corresponding to a specified conductance value x ; y_0 is the parameter for the base of the Gaussian fit; A is the parameter for the amplitude of the Gaussian fit, x_c is the parameter for the center of the Gaussian fit; and w is the parameter for the full width at half maximum for the Gaussian Fit.

5 Conductance Modulation of DNA:RNA Hybrid via Intercalation

5.1 Preparation of DNA

Single stranded DNA (ssDNA) and single stranded RNA (ssRNA) were ordered from Bio-Synthesis Inc. Arriving in solid form they are dissolved in distilled water that is filtered through a 20 nm filter (Whatman) until they reach a molarity of 300 μ M. From here the single stranded samples are split into separate Eppendorf microcentrifuge tubes of 10 μ L each and stored in a -80 C freezer (New Brunswick) until needed for hybridization.

When hybridizing, 10 μ L of single stranded DNA and RNA are mixed together in a tube with 80 μ L of filtered 100mM buffer consisting of 81 parts sodium diphosphate to 19 parts sodium monophosphate (Sigma-Aldrich), bringing the concentration of the DNA:RNA to 30 μ M. The buffer is used to halt the DNA and RNA single strands from disassociating due to repulsion from the negatively charged phosphate backbone on each.

The DNA/RNA/buffer solution is then sealed with parafilm and submerged in 1000mL of water, brought to 80 C and then allowed to cool to room temperature. This process hybridizes the single strands of DNA and RNA into a double stranded DNA:RNA hybrid. This process is a standard DNA:RNA hybridization process used in many other studies²¹.

The DNA:RNA hybrid used in this study is composed of a DNA base with sequence CCC-T9-CCC and RNA base GGG-A9-GGG both of which were purified via a high performance liquid chromatography (HPLC) protein purification method. The probe DNA has a 6-carbon spacer and amine linkers on both ends.

5.2 STM-BJ Experimental procedure

To perform the STM-BJ experiment a “substrate holder” is first cleaned using the Acetone-Methanol-Isopropanol method. The substrate holder consists of a steel plate (Figure 5.1A) with a mica stage (Figure 5.1B), three pin electrical output (Figure 5.1C), spring-loaded mounting screws (Figure 5.1D), Teflon cell (Figure 5.1F), Teflon cell mount (Figure 5.1G), and alligator clips (Figure 5.1H). In addition, there is a spring-loaded screw terminal that is used to make connection between the substrate and three-pin output (Figure 5.1E) using aluminum foil. Lastly there is the gold substrate (Figure 5.1I).

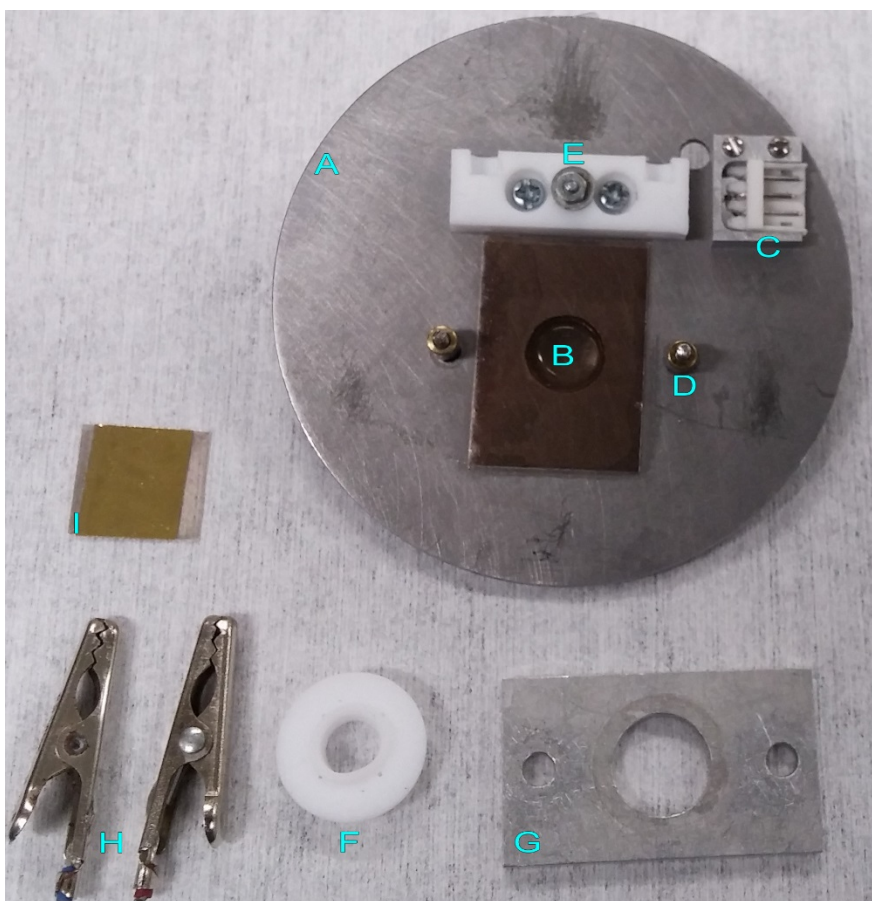


Figure 5.1: Substrate Holder Parts.

Gold substrates were prepared by first cleaving a mica surface (Ted Pella) and then evaporating 130 nm of gold (ACI Alloys, 99.999% purity) using an electron beam physical vapor

deposition under a vacuum of $\sim 10^{-7}$ Torr. Immediately after the deposition, the gold substrates underwent a temperature controlled annealing process at ~ 400 °C for ~ 5 hours under nitrogen gas using a thermal annealing process intended to smooth the gold surface and create large atomic plateaus. The gold substrates are placed individually in vials and held under vacuum for storage for use in later experiments.

After cleaning the substrate holder a gold substrate is taken from vacuum storage and annealed with a butane torch for 60 seconds to remove any remaining organic contamination as well as achieve large, atomically flat Au $\langle 111 \rangle$ surfaces. The substrate is placed on the mica stage and a thin aluminum foil strip is placed - one end under the screw terminal and the other above the substrate. The Teflon cell is loaded into the mounting screws which provide pressure on gold substrate against the aluminum foil as well as creating a reservoir where liquid sample can be placed. The assembled cell is shown in Figure 5.2.

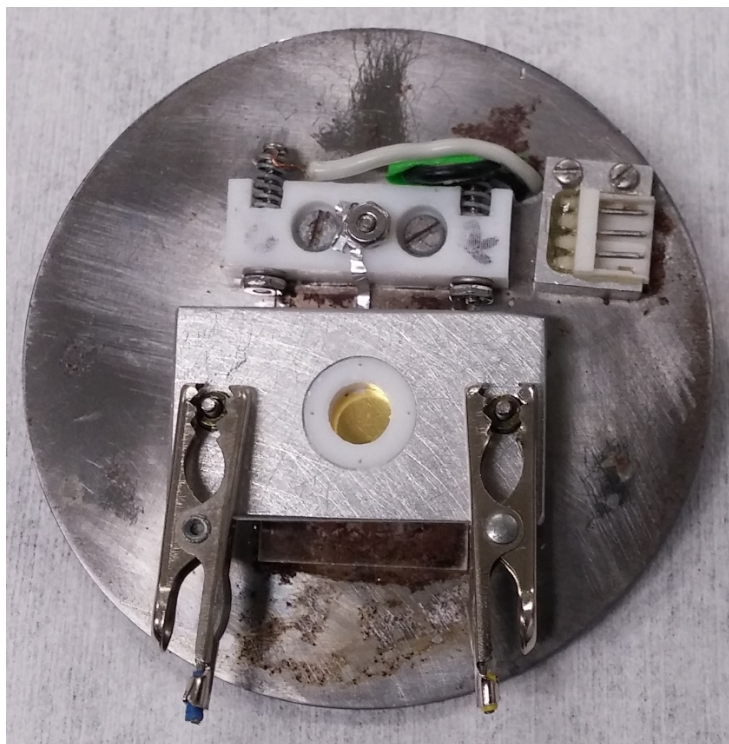


Figure 5.2: Assembled Substrate Holder

100 μ L of buffer is added to the Teflon cell reservoir in the center and contact between the substrate and three-pin output is tested with a digital multimeter using a gold wire to contact the substrate outside of the valley to avoid contamination of the buffer.

A gold tip is prepared by shearing 0.25mm diameter 99.998% pure gold wire (Alfa-Aeser) with wire cutters. The shear angle is kept as very low to increase tip sharpness. The gold tip is inspected through optical microscope and then coated in wax. The intention of coating the gold tip in wax is to expose very few atoms of gold at the end of the tip to reduce leakage current through buffer but still allow a molecular junction to form. The tip is loaded into the STM and the cell holder is mounted underneath the tip via magnetic screw posts such that the tip resides in the valley of the Teflon cell. Leakage current is checked via a LabVIEW program to ensure the buffer solution does not conduct significant current through the wax-coated tip, typically the leakage current must be below 1×10^{-5} A in order for the noise on the histogram to be located far enough away from relevant data so that conductance peaks from the target molecule can be distinguished. The STM engages a current set point of 1nA for experiments done at 10nA/V amplification and 10nA for experiments done at 100nA/V amplification. Bias is applied to the gold substrate and checked within the same LabVIEW program.

A second LabVIEW program is used to control the collection of conductance curves through the STM. A ramp rate of 20V/s is applied to the piezoelectric element to move the gold tip by increasing or decreasing this ramp rate one controls how quickly the gold tip moves towards and pulls away from the substrate; a faster ramp rate increases the movement speed of the tip which gives the molecule less time to form the junction. Current traces are viewed in real-time and saved when a 'step' is present.

After a set of control curves are collected from just buffer on the gold substrate the DNA:RNA duplex is added and given an hour of incubation time for the linkers to bind to the gold substrate. After data is collected on the duplex in buffer the intercalator complex is added at the same molarity as the duplex; this is because we expect only a single intercalator molecule to be present in each duplex due to the relative size of the intercalator to the DNA:RNA hybrid. The intercalator is given 6 to 7 hours to intercalate and current traces are then collected at the same bias/amplification parameters as the DNA:RNA duplex alone in buffer. For both the duplex and duplex plus intercalator experiments 3,000 to 6,000 current traces are collected for each applied bias; the reason for this is to ensure a large enough sample size of conductance traces such that a peak conductance value can be statistically verified through a frequency histogram. Separate biases were used at different amplification levels to more clearly see the entire range of conductance values, at the lower amplification of 10nA/V one is able to more clearly resolve the conductance region from $1 \times 10^{-6} G_0$ to around $5 \times 10^{-3} G_0$, with a higher amplification level of 100nA/V one is able to more clearly resolve the conductance region from $1 \times 10^{-4} G_0$ to around $1 \times 10^{-1} G_0$. To clearly see the shift recorded in this study both amplification levels must be used.

5.3 Results

In order to explore the intercalators effect on the DNA:RNA duplex an STM Break Junction experiment was first performed with the sequence connected to amine linkers. The results show an increase in conductance by a factor of over 500 when the intercalator molecule is present in the DNA:RNA duplex. It is important to note that a peak located near $2 \times 10^{-2} G_0$ (Figure 5.3b,d,f) is present in all experiments (even when buffer is tested without any target molecule added). An unpublished study currently in review, which was shared with Joshua Hihath's group by NJ Tao's group (Arizona State University), shows that this peak is caused by

water molecules forming a molecular junction via hydrogen bonds between the substrate and tip. The peak of interest is the one present near the $6 \times 10^{-3} G_0$ (Figure 5.3f) region which appears only after the duplex is intercalated with the intercalator complex.

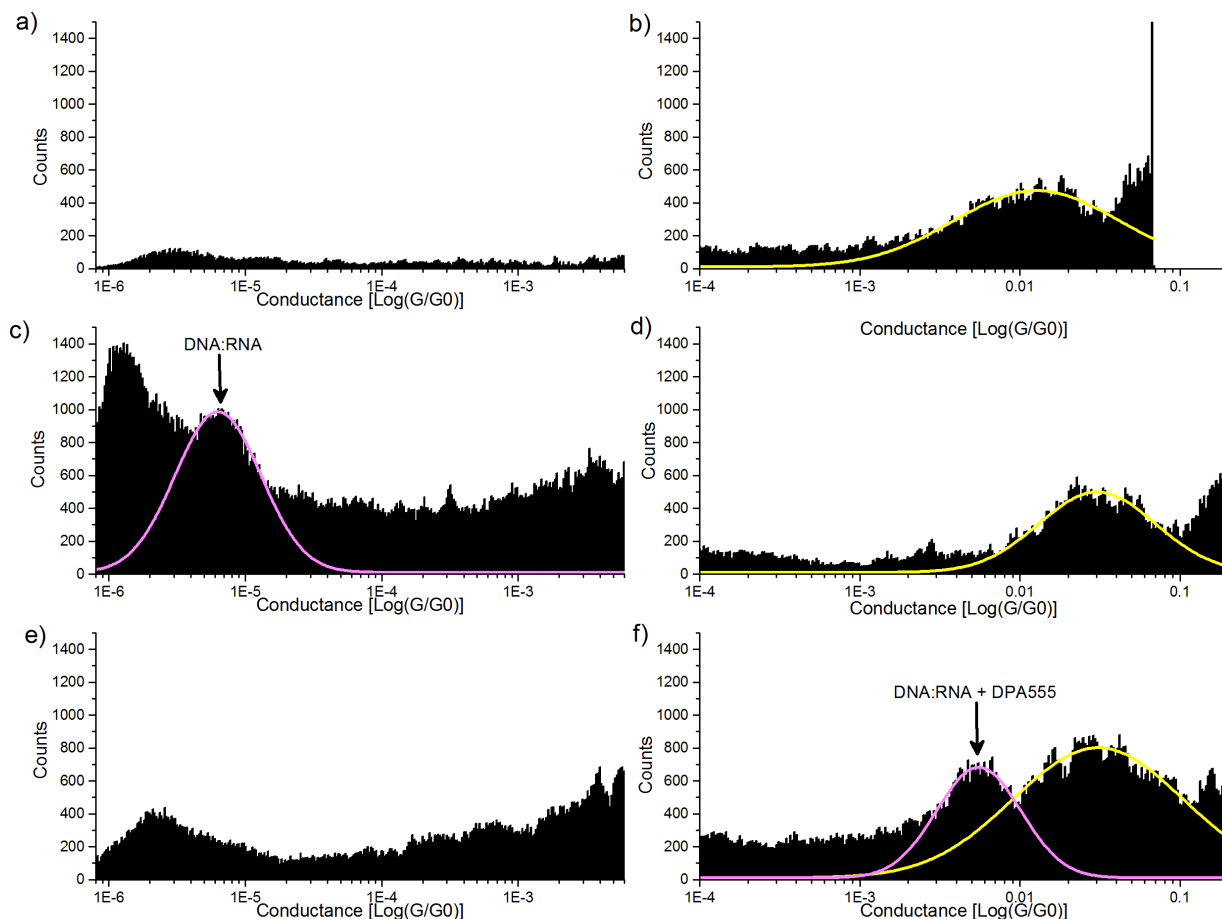


Figure 5.3: *In-Situ* intercalation of DPA555 into DNA:RNA

- a) Buffer control 200mV bias 10nA/V amplification b) Buffer control 50 mV bias 100nA/V amplification
c) DNA:RNA 200mV bias 10nA/V amplification d) DNA:RNA 50 mV bias 100nA/V amplification
e) DNA:RNA intercalated with DPA555 200mV bias 10nA/V amplification f) DNA:RNA intercalated with DPA555
50 mV bias 100nA/V amplification
Magenta fits correspond to DNA:RNA duplex with/without intercalator. Yellow fits correspond to water
conductance peak

The experiment was performed *in-situ* allowing one to see the conductance shift while the sample molecule remained the same throughout the experiment. The plots show the range of conductance values across two biases and amplifications from buffer alone (Figure 5.3a,b), to

duplex alone in buffer (Figure 5.3c,d), to the intercalator and duplex together in buffer (Figure 5.3e,f). A series of three experiments were performed under the same conditions and the resulting shift in conductance was observed and recorded. The experiments were all fit with Origin Pro 9 and the peak value of each fit were used to calculate the mean and standard deviation of the measured conductance values.

When there is no target molecule present (only buffer) only the water molecule peak near is $2 \times 10^{-2} G_0$ shown (Figure 5.3b). When the DNA:RNA duplex is alone on the substrate an experimental value of $8.325 \times 10^{-6} \pm 2.69 \times 10^{-6} G_0$ was recorded (Figure 5.3c). The high level of noise left of the conductance peak is leakage current which is only included when another peak above the leakage level is present – otherwise these curves are filtered out by the previously discussed LabVIEW program – which explains the lack of similar noise in this region in Figure 5.3a since no molecule was present at this time. After intercalation, the conductance peak in this region is no longer present (Figure 5.3e), but a new peak appears in the higher conductance region which is recorded at $4.962 \times 10^{-3} \pm 1.730 \times 10^{-3} G_0$ (Figure 5.3f). The peak in this region was not present before the intercalator was added to the sample and given time to intercalate, shown by Figure 5.3d. Conductance shift ratio is recorded by dividing the high conductance

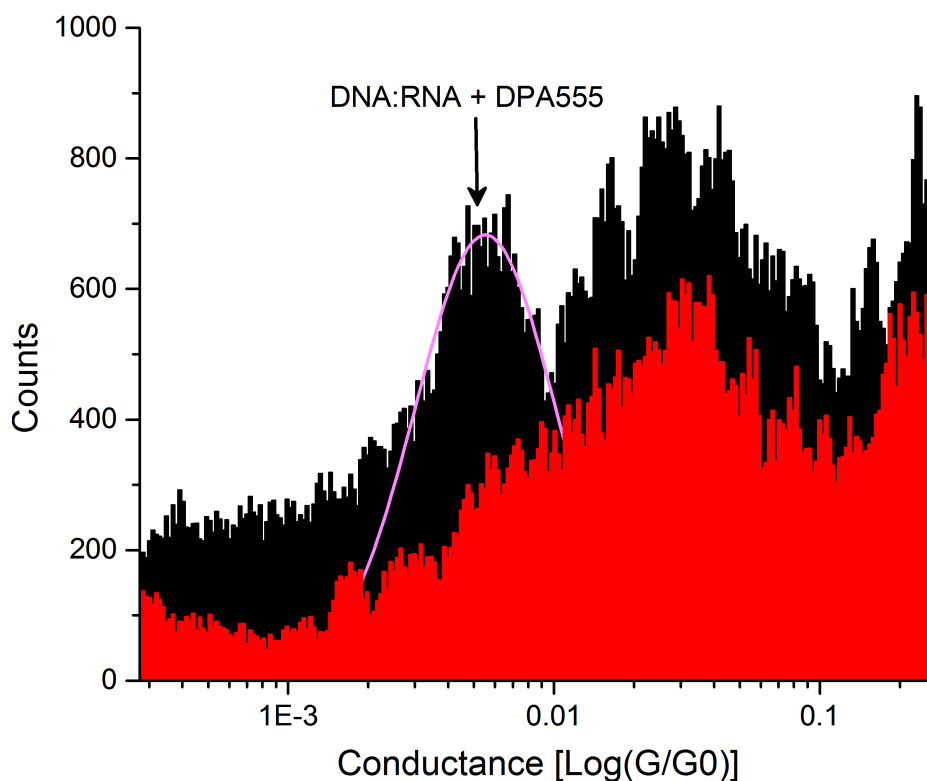
RNA:DNA+DPA555 peak in Figure 5.3f by the lower conductance for just the DNA:RNA in

Figure 5.3c. Error is propagated using $\frac{\Delta z}{z} = \sqrt{\left(\frac{\Delta x}{x}\right)^2 + \left(\frac{\Delta y}{y}\right)^2}$ where z is the conductance shift

ratio, x and y are the conductance values with respective standard deviation Δx and Δy , and Δz is the error in conductance shift ratio. Using these a conductance shift factor of 596.03 ± 283.31 .

Control experiments were performed to eliminate suspicions that the conductance shift is due to other means. First a control was done by simply adding the intercalator molecule to a cell with buffer and substrate but no DNA:RNA duplex present for it to bind to. Due to the number

of amine groups present on neomycin it is possible that the intercalator itself binds to the gold and forms a molecular junction with the STM. In such a process the duplex would take no part in charge transport and instead charge is transported through only the neomycin half of the intercalator conjugate. When conductance measurements were done on the isolated intercalator in buffer we see only a conductance peak in the low $1 \times 10^{-2} G_0$ (Figure 5.4) conductance region. The lack of any other conductance peak suggests that the high conductance peak present in the intercalated duplex sample is not caused by lone intercalators transporting through just the neomycin but instead the intercalators interaction with the DNA:RNA duplex.



*Figure 5.4: DPA555 alone in buffer collected at 50mV 100nA/V amplification
Intercalated DNA:RNA high conductance region (black) compared to the control experiment of
DPA555 alone in buffer (red). Water peak is present in both. The intercalated DNA:RNA shows additional
conductance peak.*

A second control experiment was performed to ensure that charge transport was primarily through the duplex π -stack, as opposed to the amine groups on the neomycin. The same probe DNA sequence was ordered without amine linkers and thus disabling the formed duplex from binding to the gold itself. The non-linking duplex was intercalated with the same procedure and conductance values were measured. Just as with the lone intercalator control, this experiment yielded a single conductance peak in the low $1 \times 10^{-2} G_0$ (Figure 5.5) region which suggests that transport is not taking place in the target molecule without the presence of linker groups on the duplex to facilitate transport through the π -stack. This control experiment was collected at 20mV bias which explains why the leakage current noise can be seen in the $1 \times 10^{-4} G_0$ region.

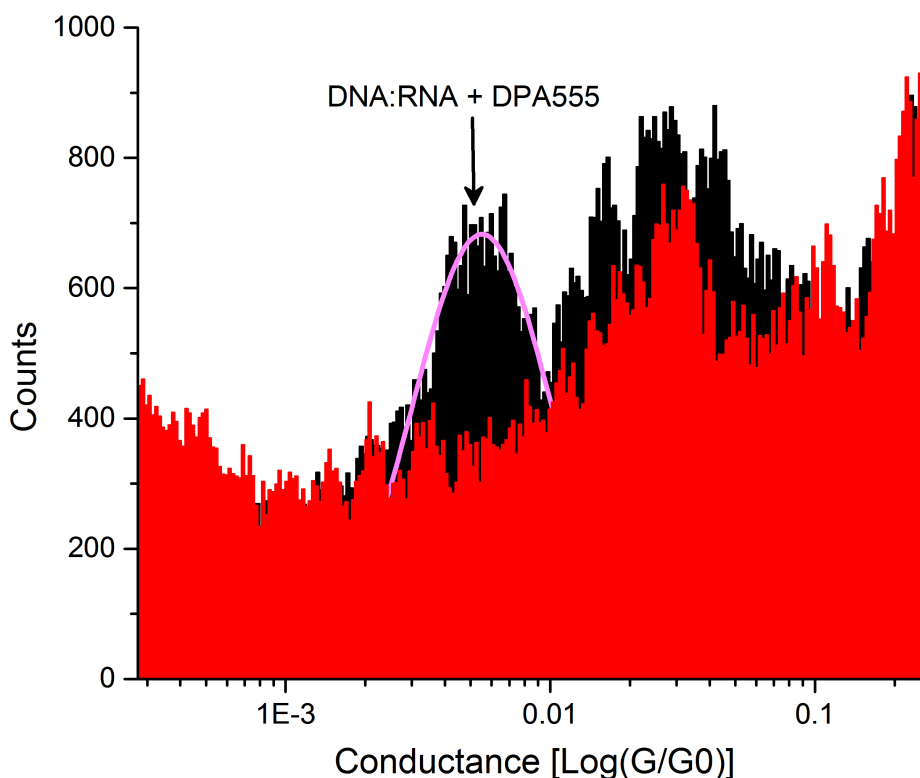


Figure 5.5: DNA:RNA without linkers collected at 20mV bias 100nA/V amplification Intercalated DNA:RNA high conductance region (black) compared to the control experiment of intercalated DNA:RNA without amine linkers (red). Water peak is present in both. The intercalated DNA:RNA with linkers shows additional conductance peak.

Although the experiments were not collected at the same bias voltage this does not affect the comparison between molecular conductance values as one can see the water peak is constant regardless of the bias used to collect the current traces and calculate conductance values. This noise is present in all experiment but shifts depending on the applied voltage, unlike the conductance peaks which are fixed.

These results, intuitively, makes sense because the neomycin – although having the ability to form a molecular junction due to the many amine groups present – is a large molecule with only saturated pathways, thus even if we could detect the presence of transport through the molecule, we would expect the conductance to be very small. This is because carriers are able to be transported through unsaturated pathways much more easily than through saturated ones due to the double or triple bonds on unsaturated paths which increase molecular orbital overlap. In Neomycin, the bonds present are all saturated – only having carbon-carbon single bonds – making carrier transport more difficult.

The significant increase in conductance could be caused by a few possible changes in the transport mechanisms dominant in the system. The first reasonable explanation for the shift is a large delocalization of the π -stack density of states. In studies²² which model the electron density of DNA systems there is often large localization around the base pairs, thus delocalization is a strong possibility when introducing anthraquinone which disrupts the π -stack. The anthraquinone is embedded directly into the base pair stack of the duplex which can disrupt the local density of states causing it to spread out further over the length of the duplex creating large overlap in the molecular orbitals. A delocalization in the density of states along the π -stack can make it easier for hopping to occur by rearranging the energy of the states available and potentially lowering them into a more favorable region for hopping, in addition delocalization encourages tunneling

in the system which produces a higher likelihood of coherence corrected hopping as described in Section 2.3.3.

The second explanation for the large increase is due to additional hopping sites that may be added by the intercalator. The intercalator may add additional hopping sites at energies close to the fermi energy of gold. If this were the case, then we could expect an increase in the rate of hopping as the energy alignment of the new sites make the transitions more favorable. This system is depicted in Figure 5.6.

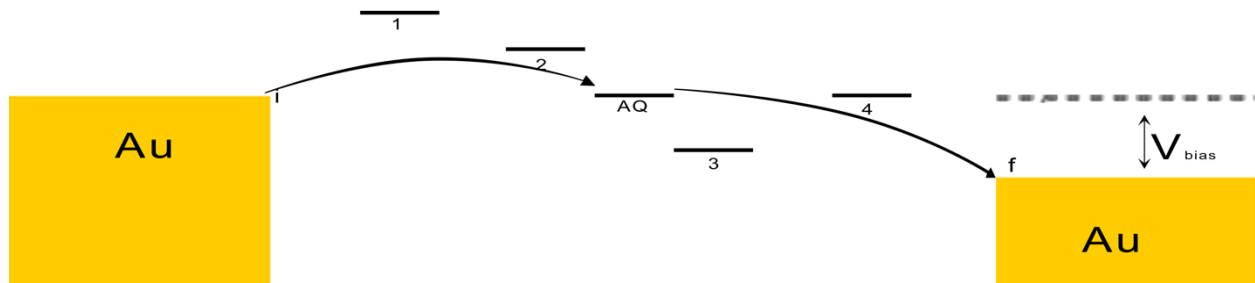


Figure 5.6: Energy sites after intercalation.

A possible reason for the increased conductance is a newly introduced energy state very close to the gold fermi energy allowing for an easier transition to this site instead of the first site since the energy barrier to this site is less than the first few bridge sites required energy..

Transitions directly from one gold electrode to the energy site introduced by the anthraquinone and then to the other electrode may become the dominant transport method, ignoring many of the intermediate bridge sites that were previously used for transport and instead ‘skipping over them’ to the newly introduced site which is close in energy. Mott variable range hopping is a model which can describe this system as it abandons the nearest neighbor assumption of the hopping model previously introduced and allows for carriers to hop to sites which are not only close by, but energetically favorable. In this manner, a carrier will jump to a further bridge site if the closer ones would require too much additional energy.

6 Redox Properties of Intercalated DNA:RNA Hybrid

As mentioned in section 3, anthraquinone is a redox active molecule containing two oxygens. It has already been shown that gating an anthraquinone based molecule is possible to achieve switching-like behavior, though none have combined anthraquinones switching behavior with its intercalating effect to produce a DNA-based device.

To further explore the properties of the intercalator on the duplex a series of electrochemical experiments were performed using a Gamry Instruments Reference 600 potentiostat. A sample of the duplex was incubated with the intercalator and immobilized onto a gold substrate in the same type of phosphate buffer as used for the STM Break Junction experiments for 24 hours. Both cyclic voltagrams as well as square wave voltagrams were used to measure the redox potential of the intercalated duplex molecule.

The cyclic voltagram (Figure 6.1) shows a clear reduction peak around -500 mV but no obvious oxidation. The downward slope around zero suggests a possible, although very weak, oxidation signal that is hard to detect. In addition the fact that the signal shows a 'dip' during the positive direction voltage sweep (the higher current feature near -500 mV) suggests that it is difficult to fully reduce many of the molecules on the surface which may be indicative of an irreversible or difficult-to-reverse reduction process; thus one might need to apply potentially large gate voltages to get switching behavior from the intercalated DNA:RNA.

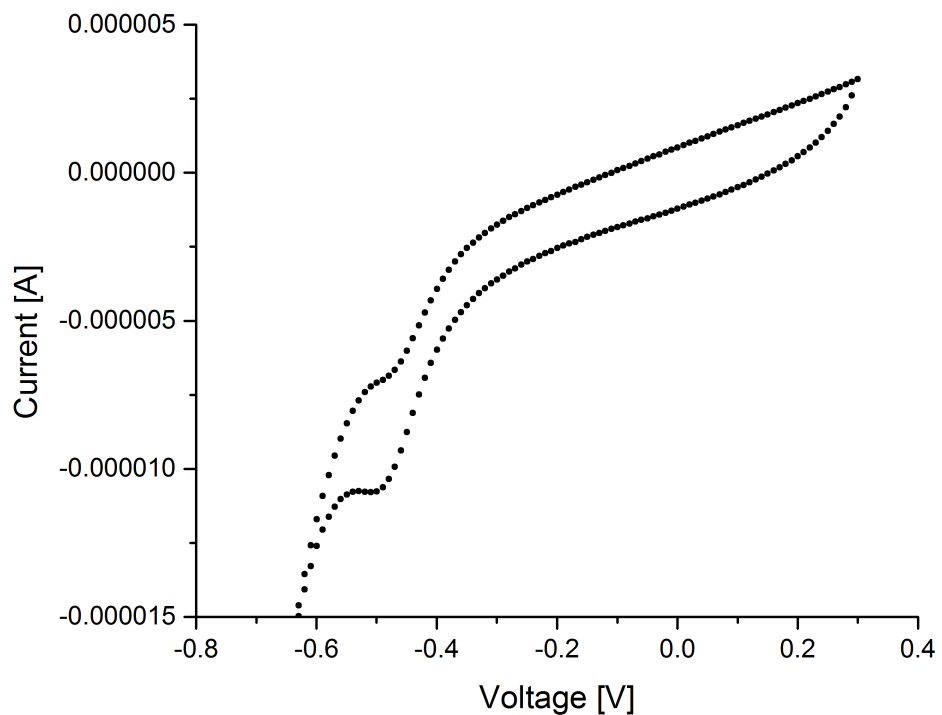


Figure 6.1: Cyclic Voltammogram of DPA555 intercalated DNA:RNA duplex.

Square wave voltammetry was performed as an additional way to probe the reduction and oxidation potentials of the subject molecule. The results of the square wave voltammetry show a very large peak near -500 mV (Figure 6.2) which confirms that the redox properties of the intercalated duplex are dominated by reduction.

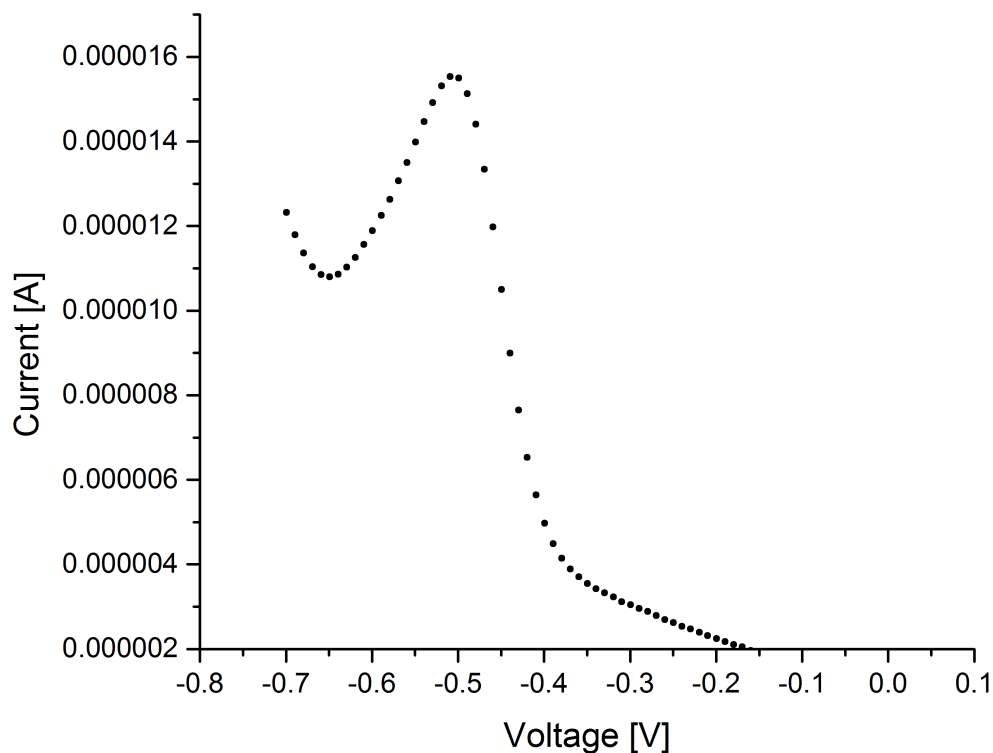


Figure 6.2: Square Wave Voltogram of DPA555 intercalated DNA:RNA duplex

These results suggest that it is possible to alter the reduction and oxidation states of the anthraquinone while it is intercalated in between the base pairs of the DNA:RNA duplex but also indicate gating between the two states may be difficult.

A control was performed to understand how intercalation in the duplex affected the redox potentials of the anthraquinone by allowing just a sample of the intercalator in buffer to bind to a gold substrate and then performing a cyclic voltogram. The resulting plot (Figure 6.3) shows clear oxidation and reduction potentials that are shifted from what is seen in the intercalated duplex; the reduction peak is located at -200mV and the oxidation peak is located around 0mV. This indicates that the effect of the intercalator binding to the DNA:RNA not only cause a significant shift in the reduction peak from -500mV to -200mV but also stifles the oxidation peaks signal significantly. In addition, the lack of secondary ‘dip’ in the reduction region

indicates that the binding to the DNA:RNA hybrid causes some of the difficulties fully reducing and oxidizing the anthraquinone.

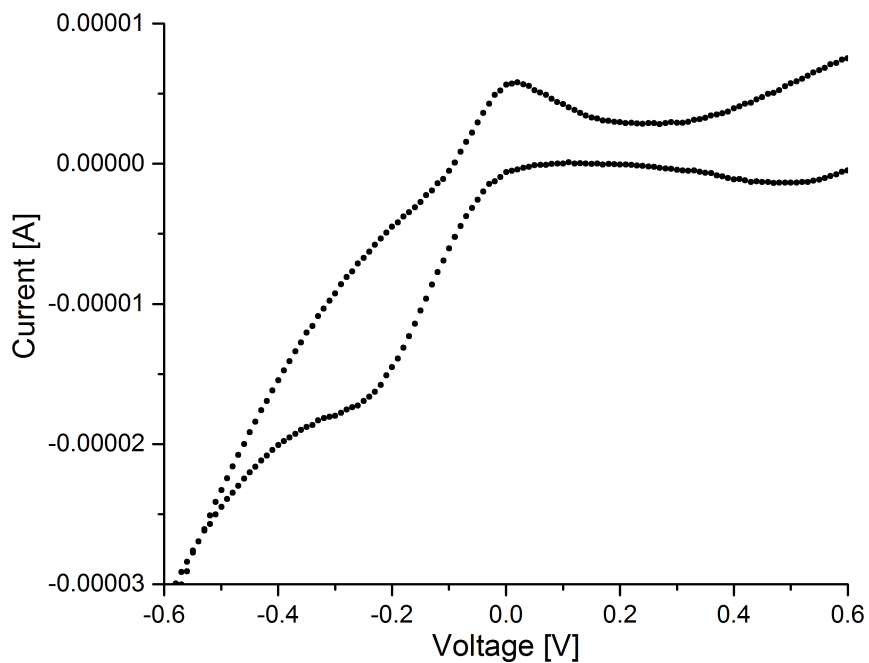


Figure 6.3: Cyclic Voltammogram of DPA555 alone

These redox states are promising for their potential to manipulate the energy of the states via electrochemical gating and alter the hopping pathway for carriers through the system. By altering hopping pathways one could potentially see a change in the conductance depending on whether the states are reduced or oxidized, this possibility is discussed in the next section.

7 Conclusion and Outlook

In conclusion, this study explored the effect of the anthraquinone-neomycin conjugate intercalator on the conductance of a DNA:RNA duplex. Using the robust and well established Scanning Tunneling Microscope Break Junction technique to probe the conductance of single molecule junctions current traces were collected and analyzed. The results show a significant increase in the conductance due to the effect of the intercalating agents interaction with the DNA:RNA hybrid duplex π -stack. In addition, possible transport models were discussed as likely candidates to explain the large increase in conductance. The redox potentials of the intercalated structure were explored via electrochemical experiments which revealed a possibility for electrochemical gating of the system.

Looking forward there are many recommendations for future study of this intercalators interaction with DNA:RNA duplexes. To further understand which model is most appropriate to describe the transport of the intercalated duplex one can perform length-dependence experiments where DNA:RNA sequences of varying numbers of base pairs are tested with the same intercalator to determine which transport model describes the system most accurately.

Moreover, much can be done to explore the structural effects of the intercalator on the duplex. Circular Dichroism (CD) Spectroscopy experiments can be performed to understand how the intercalator changes the structure of the duplex by unwinding it to create room or the intercalator to bind, and Molecular Dynamics simulations can be performed to identify how the intercalator causes preferential binding to specific base pairs.

In addition, by using a bipotentiostat one can apply a gate voltage to perform STM Break Junction experiments whilst actively forcing the intercalator into either a reduced or oxidized state to further study the effect that the redox-active anthraquinone has on the conductance. It is

possible that using a gate electrode one can modulate the conductance through the π -stack by changing the energy level of the additional anthraquinone site. For instance, consider a scenario wherein the energy level of the anthraquinone is significantly lowered while it is in the reduced state (depicted in Figure 7.1), in such a system the carrier may preferentially hop over the site entirely thus returning to the original hopping transport it had before the introduction of the intercalator.

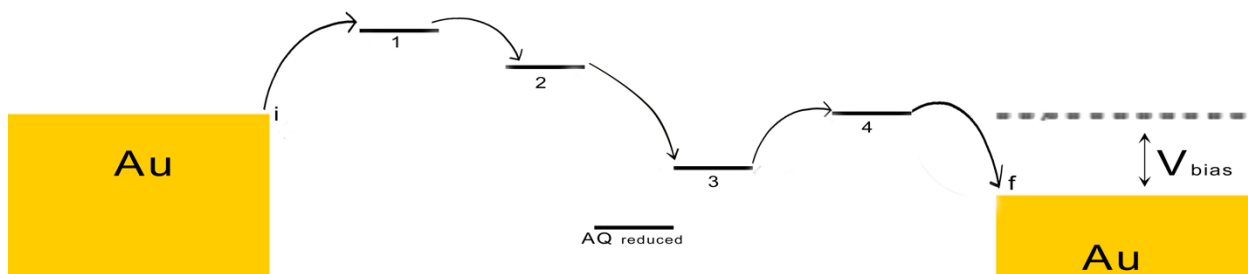


Figure 7.1: Possible state resulting from gating intercalated duplex. Gating to force anthraquinone into reduced state may change the energy of the additional site to return the duplex to its original conductance.

Doing so could potentially allow for powerful transistor-like switching behavior if the gating returns the DNA:RNA duplex to near its original low-conductance state.

Lastly, many novel applications of these intercalators can be applied to future experiments in biosensing and molecular electronics. Being able to reliably gate a molecular device has long been a goal of this still-emerging field of molecular electronics and will lead us towards new devices in both computing applications and healthcare. DNA and RNA structures have been identified for their unique ability to self-assemble as well as their vital importance in biological processes and by further exploring how these intercalator structures interact with single strand, duplex, and even higher order systems such as those made via DNA origami we may soon achieve reliable molecular devices that can be incorporated into a variety of systems.

8 References

- ¹ Lee, H., Yu, S.W., Ryu, J.W. Han, K. Jeon, D.Y. Jang, K.H. Kim, J. Lee, J.H. Kim, S. Jeon, G. Lee, J. Oh, Y. Park, W. Bae, J. Yang, J. Yoo, S. Kim, and Y.K. Choi. "Sub-5nm All-Around Gate FinFET for Ultimate Scaling." 2006 Symposium on VLSI Technology, Digest of Technical Papers. (2006).
- ² Hush, Noelle S. "An Overview of the First Half-Century of Molecular Electronics." *Annals of the New York Academy of Sciences* 1006.1 (2003): 1-20
- ³ Aviram, Arieh; Ratner, Mark A. "Molecular Rectifiers". *Chemical Physics Letters*. 29 (1974): 277–283.
- ⁴ Aviram, Arieh. "Molecules for memory, logic, and amplification." *Journal of the American Chemical Society* 110 (1988):5687-5692
- ⁵ Carter, F.L, Siatkowski, R.E., Wohltjen, H. *Molecular Electronic Devices: Proceedings of the 3. International Symposium, Arlington, Va. 1986.* Amsterdam: North-Holland, (1988).
- ⁶ Joachim, Christian, James K. Gimzewski, Reto R. Schlittler, and Corinne Chavy. "Electronic Transparency of a Single C 60 Molecule." *Physical Review Letters* 74.11 (1995): 2102-105
- ⁷ Rothemund, Paul W. K. "Folding DNA to Create Nanoscale Shapes and Patterns." *Nature* 440.7082 (2006): 297-302.
- ⁸ Aldaye, F. A., Palmer, A.L., and H. F. Sleiman. "Assembling Materials with DNA as the Guide." *Science* 321.5897 (2008): 1795-799.
- ⁹ Endres, R. G., D. L. Cox, and R. R. P. Singh. "Colloquium : The Quest for High-conductance DNA." *Reviews of Modern Physics* 76.1 (2004): 195-214.
- ¹⁰ Eley, D. D., and D. I. Spivey. "Semiconductivity of Organic Substances. Part 9.—Nucleic Acid in the Dry State." *Trans. Faraday Soc.* 58.0 (1962): 411-15
- ¹¹ Linko, Veikko, Ari Ora, and Mauri A. Kostiainen. "DNA Nanostructures as Smart Drug-Delivery Vehicles and Molecular Devices." *Trends in Biotechnology* 33.10 (2015): 586-94.
- ¹² Guo, Cunlan, Kun Wang, Zerah-Harush, Elinor, Hamill, Joseph , Wang, Bin, Dubi, Yonatan and Bingqian Xu. "Molecular Rectifier Composed of DNA with High Rectification Ratio Enabled by Intercalation." *Nature Chemistry* 8.5 (2016): 484-90.
- ¹³ Kershner, Ryan J., Luisa D. Bozano, Christine M. Micheel, Albert M. Hung, Ann R. Fornof, Jennifer N. Cha, Charles T. Rettner, Marco Bersani, Jane Frommer, Paul W. K. Rothemund, and Gregory M. Wallraff. "Placement and Orientation of Individual DNA Shapes on Lithographically Patterned Surfaces." *Nature Nanotechnology* 4.9 (2009): 557-61.
- ¹⁴ Gally, Tom. "Diagram of HOMO and LUMO molecular orbitals." (2010).
- ¹⁵ Landauer, R. "Spatial Variation of Currents and Fields Due to Localized Scatterers in Metallic Conduction". *IBM Journal of Research and Development*. 1 (1957): 223–231.
- ¹⁶ Nazarov, Y. V. Blanter, Ya. "Quantum transport: Introduction to Nanoscience." Cambridge University Press. (2009): 29–41
- ¹⁷ Diederichsen, U. "Charge Transfer in DNA: A Controversy." *Angewandte Chemie International Edition* 36 (1997): 2317-2319
- ¹⁸ Geneaux, J. C., Barton, J. K. "Mechanisms for DNA charge transport." *Chemical Reviews* 110 (2009): 1642–1662
- ¹⁹ Bixon, M., B. Giese, S. Wessely, T. Langenbacher, M. E. Michel-Beyerle, and J. Jortner. "Long-Range Charge Hopping in DNA." *Proceedings of the National Academy of Sciences* 96.21 (1999): 11713-1716.
- ²⁰ Xu, Zhang, Li, and Tao. "Direct Conductance Measurement of Single DNA Molecules in Aqueous Solution." *Nano Letters* 4.6 (2004): 1105-108

-
- ²¹ Li, Yuanhui, Juan M. Artés, Jianqing Qi, Ian A. Morelan, Paul Feldstein, M. P. Anantram, and Joshua Hihath. "Comparing Charge Transport in Oligonucleotides: RNA:DNA Hybrids and DNA Duplexes." *The Journal of Physical Chemistry Letters* 7.10 (2016): 1888-894.
- ²² Artés, Juan Manuel, Yuanhui Li, Jianqing Qi, M. P. Anantram, and Joshua Hihath. "Conformational Gating of DNA Conductance." *Nature Communications* 6 (2015): 8870
- ²³ Li, Ling. "Charge Transport in Organic Semiconductor Devices." *Advances in Polymer Science* Volume 223 (2009). 301-323
- ²⁴ Marcus, Rudolph A. "On the Theory of Oxidation-Reduction Reactions Involving Electron Transfer. I." *The Journal of Chemical Physics* 24.5 (1956): 966.
- ²⁵ Asadi, Kamal, Auke J. Kronemeijer, Tobias Cramer, L. Jan Anton Koster, Paul W. M. Blom, and Dago M. De Leeuw. "Polaron Hopping Mediated by Nuclear Tunnelling in Semiconducting Polymers at High Carrier Density." *Nature Communications* 4 (2013): 1710.
- ²⁶ Buttiker, M. "Coherent and Sequential Tunneling in Series Barriers." *IBM Journal of Research and Development* 32.1 (1988): 63-75.
- ²⁷ Richards, A. D.; Rodgers, A. "Synthetic metallomolecules as agents for the control of DNA structure". *Chemical Society Reviews*. 36.3 (2007): 471–83.
- ²⁸ Lerman, L. S. "Structural considerations in the interaction of DNA and acridines". *Journal of Molecular Biology*. 3.1 (1961): 18–30.
- ²⁹ Wang, Xiaolong, Li Gao, Bo Liang, Xin Li, and Xuefeng Guo. "Revealing the Direct Effect of Individual Intercalations on DNA Conductance toward Single-molecule Electrical Biodetection." *Journal of Materials Chemistry B* 3.26 (2015): 5150-154.
- ³⁰ Arya, Dev P., Liang Xue, and Bert Willis. "Aminoglycoside (Neomycin) Preference Is for A-Form Nucleic Acids, Not Just RNA: Results from a Competition Dialysis Study." *Journal of the American Chemical Society* 125.34 (2003): 10148-0149.
- ³¹ Walter, Frank, Quentin Vicens, and Eric Westhof. "Aminoglycoside–RNA Interactions." *Current Opinion in Chemical Biology* 3.6 (1999): 694-704.
- ³² Xi, Hongjuan, David Gray, Sunil Kumar, and Dev P. Arya. "Molecular Recognition of Single-Stranded RNA: Neomycin Binding to Poly(A)." *FEBS Letters* 583.13 (2009): 2269-275.
- ³³ Shaw, Nicholas N., Hongjuan Xi, and Dev P. Arya. "Molecular Recognition of a DNA:RNA Hybrid: Sub-nanomolar Binding by a Neomycin–methidium Conjugate." *Bioorganic & Medicinal Chemistry Letters* 18.14 (2008): 4142-145.
- ³⁴ Dijk, Elisabeth H. Van, Daniel J. T. Myles, Marleen H. Van Der Veen, and Jan C. Hummelen. "Synthesis and Properties of an Anthraquinone-Based Redox Switch for Molecular Electronics." *Organic Letters* 8.11 (2006): 2333-336.
- ³⁵ Yang L1, Fu Z2, Niu X, Zhang G, Cui F, Zhou C. "Probing the interaction of anthraquinone with DNA by spectroscopy, molecular modeling and cancer cell imaging technique." *Chemico-Biological Interactions* 233 (2015): 65-70
- ³⁶ Binnig, G.; Rohrer, H. "Scanning tunneling microscopy". *IBM Journal of Research and Development*. 30.4 (1986): 355–69.
- ³⁷ Chen, J.; "Introduction to Scanning Tunneling Microscopy." Oxford University Press. (1993).
- ³⁸ Schmid, Michael. "The Scanning Tunneling Microscope." [IAP/TU Wien]. Institut Für Angewandte Physik, 23 Nov. 2011.
- ³⁹ Xu, B., Tao, N. J. "Measurement of Single-Molecule Resistance by Repeated Formation of Molecular Junctions." *Science* 301 (2003):1221-1223
- ⁴⁰ Hihath, Joshua, and Nongjian Tao. "The Role of Molecule–electrode Contact in Single-molecule Electronics." *Semiconductor Science and Technology* 29.5 (2014).